Molten-Salt Flux Mediated Synthesis of ZnO-SnO_2 composites: Effects of Surface Areas and Crystallinities on Photocatalytic Activity

Rachelle Austin[1], Feier Hou*[2]

Department of Chemistry, Western Oregon University

Abstract

ZnO-SnO_2 composites have been found to demonstrate photocatalytic activities. In this study, ZnO-SnO_2 composites were synthesized using flux synthesis, a synthetic approach different from previous studies, in which molten $ZnCl_2$ acted both as a reactant and as the flux for the reaction. Their photocatalytic properties were measured for the degradation of the organic dye, methylene blue. It was found that as the temperatures of the synthesis increase, the specific surface areas of the ZnO-SnO_2 composites decrease, which would decrease their photocatalytic activities due to decreased adsorption of the dye on the surface of the composites; while their crystallinity increases, which would increase their photocatalytic activities due to the smaller concentration of defects and thus improved mobility of the charge carriers. An interplay of those two factors affects their photocatalytic activities, with the composite with the highest photocatalytic activity degrading approximately 95% of the methylene blue dye within 10 minutes. By changing the temperature of the flux synthesis alone, the crystallinity and surface area of the ZnO-SnO_2 composite can be changed, which provides a possible way to obtain ZnO-SnO_2 composites with relatively high crystallinity and surface area to maximize their photocatalytic activity.

1. Introduction

Organic pollutants have become one of the overwhelming problems of the world with growing industrialization and population. One family of organic pollutants are organic dyes, which often come from the textile industry, household products, or personal care products. The release of organic dyes as wastewater are presently of great concern, because they may be toxic, carcinogenic and mutagenic; meanwhile, their complete biodegradation is often very slow, which affects sunlight penetration and photosynthesis.[1] Photocatalytic degradation, in which a catalyst is used to speed up the degradation of organic dyes under light irradiation, is often viewed as the "green" approach for the degradation of organic dyes into nontoxic products. A variety of semiconducting materials, such as TiO_2 and some ternary oxides, have been reported as photocatalysts for the degradation of organic dyes.[2-10]

ZnO-SnO_2 composites have been found to demonstrate photocatalytic activities for the degradation of several different organic dyes under UV and visible light irradiation.[11-32] Pure ZnO also demonstrate photocatalytic activity[11,33], while pure SnO_2 shows only little photocatalytic activity, likely due to the fast recombination of the photogenerated electron/hole pairs.[11,14,23] The conduction band of SnO_2 is lower than that of ZnO, so that it can act as the sink for the photogenerated electrons from ZnO; moreover, the photogenerated positive holes in the valence band of SnO_2 can move to the valence band of ZnO, which leads to more efficient charge separation and less electron-hole recombination, and results in increased photocatalytic activities in ZnO-SnO_2 composites.[11,14,17-19,26,28,29,34,35] Furthermore, the sizes of the particles in ZnO-SnO_2 composites are often small, with most of them being nanomaterials[12-16,18,21,23-25,28,29,34] and

[1] Now at Department of Chemistry, Colorado State University

[2] houf@wou.edu

some being porous[19,21,34], which leads to increased surface area and thus increased photocatalytic activities.[11,23]

In this study, we present ZnO-SnO_2 composites prepared by flux synthesis at different temperatures. The flux synthetic method is a modification of the high-temperature solid state ceramic synthetic method. In a flux synthesis, a selected inorganic salt is made molten by being heated above its melting point, which acts as a solvent to dissolve the solid reactants in the synthesis and for crystallization of the products. Compared to other synthetic methods, the flux synthesis has several advantages, such as shortening the reaction time and lowering the reaction temperature by improving the diffusion rate of the reactants, facilitating crystal growth with improved morphology and particle size homogeneity, and manipulating particle sizes and morphologies[36-43]. Therefore, the molten salt flux-mediated method provides a straight-forward way to synthesize ZnO-SnO_2 composites with the possibility to tune the crystallite sizes and crystallinities of the composite by varying synthetic conditions such as the temperature. To our best knowledge, this is the first time the ZnO-SnO_2 composite has been prepared using the flux method. The composites synthesized at different temperatures demonstrate varied photocatalytic activities for the degradation of methylene blue, which will be discussed in terms of their surface areas and crystallinities related to the synthetic temperatures.

2. Experimental

2.1 Materials

$ZnCl_2$, $BaCO_3$, and ZnO (reagent grade) were purchased from Flinn Scientific. SnO_2 (purity: ≥ 99.9%) was purchased from Beantown Chemical. $AgNO_3$ (purity: ≥ 99.9%) was purchased from Cynmar Coorperation. All starting materials were used without further purification.

2.2 Synthesis of ZnO-SnO_2 composites

First, Ba_2SnO_4 was synthesized by heating $BaCO_3$ and SnO_2 at 2:1 molar ratio in air inside a muffle furnace at 900 °C for 48 h, according to the literature method[44]. The purity of the as-synthesized Ba_2SnO_4 was confirmed by powder X-ray diffraction (PXRD), and was then grinded with $ZnCl_2$ in a 1:2.5 molar ratio in an agate mortar with pestle. The grinded mixture was then transferred to an alumina crucible, heated to a reaction temperature of 400, 500, 600, 700, 800, and 900 °C, respectively, at a heating rate of 5 °C/min, and held at the reaction temperature for 24 h before cooling back down to room temperature. During the synthesis, $ZnCl_2$ acted both as a reactant and as the molten salt flux to dissolve the other reactant and facilitate crystallization of the products. The resulting light yellow (500 °C) or white (all other temperatures) powder was washed with DI water until no Cl^- was left (confirmed by adding 0.100 *M* $AgNO_3$ solution to the decantant), and dried in air at room temperature.

2.3 Characterization

PXRD patterns were obtained on a Rigaku R-Axis Spider using Cu $K_{\alpha 1}$ radiation (λ=1.54056 Å) from a sealed tube X-ray source (40 kV, 36 mA) and a curved image-plate detector. Mid-infrared (400-4000 cm^{-1}) spectra were measured on an IR-Prestige 21 Shimadzu Fourier transform infrared spectrophotometer (FTIR) equipped with a GladiATR accessory. Approximately 5 mg of powder was loaded onto the sample stage, and the data were plotted as transmittance versus wavenumber. Bandgap energies were measured by UV-vis diffuse reflectance spectra using a Shimadzu UV-3600/3100 UV-vis-NIR spectrophotometer equipped with an integrating sphere. A pressed barium sulfate powder tablet was used as the reference. The data were transformed using the Kubelka – Monk function, F(R).[45] Tauc plots were plotted as $(F(R)h\nu)^2$ versus energy ($h\nu$). The optical bandgap energies were estimated from the

inflection point tangent to the linear portion of the absorption curve.[46] Scanning electron microscopy (SEM) images and elemental analyses was performed using an FEI Verios 460L field emission scanning electron micro-scope (FESEM) equipped with an Oxford energy dispersive X-ray spectrometer (EDS). Specific surface areas were determined using a Quantachrome ChemBET Pulsar TPR/TPD. Each sample was degassed by heating to 250 °C under flowing N_2 for 4 h, then cooled with liquid N_2, and analyzed using a 30% He/N_2 mixture.

2.4 Photocatalytic Organic Dye Degradation

For each $ZnO\text{-}SnO_2$ composite, a 30 mg sample was added to a 35 mL solution of 1.0×10^{-5} M of methylene blue (MB) in a quartz glass tube. The suspension was magnetically stirred in the dark for ~20 min to ensure adsorption equilibrium and uniform dispersity. The mixture was then irradiated by a Xe arc lamp with a photon flux of ~200 mW/cm^2, while being magnetically stirred at room temperature. The Xe arc lamp was equipped with an IR filter, and emits both ultraviolet ($\lambda > 230$ nm) and visible ($\lambda > 400$ nm) light. Every 10 minutes, approximately 4 mL of the mixture was withdrawn and placed on the lab bench for the solid powder to precipitate to the bottom. Absorbance of the clear liquid was then measured using a Shimadzu UV-3600/3100 UV-vis-NIR spectrophotometer to monitor the change in concentration of MB during the dye degradation process. After 60 minutes, the reaction mixture was removed from the irradiation of light, and the solid was recovered by centrifugation. PXRD patterns were taken on each recovered solid sample and compared to the PXRD patterns of the as-prepared solid samples to test for any structural changes during the dye degradation process.

As control experiments, the same procedure was performed on the same MB solution under light irradiation without any $ZnO\text{-}SnO_2$ composite, as well as on the same MB solution with $ZnO\text{-}SnO_2$ composite synthesized at 500 °C without light irradiation. To verify that the composites obtained are actually composites instead of simple phase mixtures, the same procedure was also performed on pure ZnO and pure SnO_2, each heated to 500 °C for 24 hours under the same heating procedure as in the syntheses of the composites, as well as on a simple mixture of ZnO and SnO_2 (2.5:1 molar ratio) that was also heated to 500 °C for 24 hours under the same heating procedure as in the syntheses of the composties.

3. Results and Discussion

3.1 Synthesis and Characterizations

The synthetic method was originally designed for the synthesis of Zn_2SnO_4 using the reaction: $Ba_2SnO_4 + 2ZnCl_2 \rightarrow Zn_2SnO_4 + 2BaCl_2$. An excess amount of $ZnCl_2$ was added into the starting materials ($n(ZnCl_2)$: $n(Ba_2SnO_4) = 2.5:1$, instead of 2:1 as indicated by the stoichiometry) to ensure complete reaction of Ba_2SnO_4. However, since the synthesis was performed in air, the resulting Zn_2SnO_4 likely decomposed into ZnO and SnO_2, leading to an overall reaction: $Ba_2SnO_4 + 2ZnCl_2 \rightarrow 2ZnO + SnO_2 + 2BaCl_2$. All syntheses were performed above the melting point of $ZnCl_2$ (290 °C), thus $ZnCl_2$ acted both as a reactant and as a flux to accelerate the diffusion rate of other reactants. After the reaction, the products were washed with DI water until there was no Cl^- left to remove $BaCl_2$ and any excess $ZnCl_2$. Since the synthetic method was originally designed for the synthesis of Zn_2SnO_4, we have synthesized Zn_2SnO_4 using a hydrothermal synthesis according to the literature[47] instead, and conducted the same characterizations and measurements on it to compare to the $ZnO\text{-}SnO_2$ composites in this work.

The PXRD patterns of the composites are compared to the PXRD patterns of pure ZnO[48] and pure SnO_2[49] from literature, and the results are shown in Figure 1. The composites synthesized at 500, 600,

700, 800, and 900 °C are composed of ZnO and SnO_2. The composite synthesized at 400 °C is mostly amorphous with only one very broad peak, so it is not possible to tell its composition from its PXRD pattern. For those composites, as the temperature of the synthesis increases, the heights of the SnO_2 reflections increases, while heights of the ZnO reflections remain relatively unchanged, which indicates that the crystallinity of the SnO_2 in the composites increases while the crystallinity of the ZnO in the composites remains unchanged. The crystallinity of SnO_2 in each sample is represented by the ratio of the height of the most intense reflection of SnO_2 (Peak a in Figure 1) to that of the most intense reflection of ZnO (Peak b in Figure 1) and shown in Figure 2. For the composite synthesized at 400 °C, since the most intense reflection of SnO_2 is not present in its PXRD pattern, its crystallinity is marked as zero.

Interestingly, the color of the composite synthesized at 500 °C is slightly yellow, which is different from the composites synthesized at all other temperatures. ZnO is known to turn yellow when heated, due to a small loss of oxygen at high temperature that leads to oxygen vacancies (i.e. higher Zn to O ratio) in the ZnO lattice[50]. Since the composite synthesized at 500 °C also has lower crystallinity compared to composites synthesized at higher temperatures and the highest Zn to O ratio in its composition (as shown in Table 1), having defects is a possible cause for its light yellow color.

No peak broadening was observed on the PXRD patterns. Using the Scherrer equation[51]: $B = \frac{K\lambda}{\beta \cos\theta}$ on the most intense peak of SnO_2 (Peak a in Figure 1) in the PXRD patterns (where B is the crystallite size, the K factor is 1, λ is the wavelength of the X-ray radiation (1.54056 Å), β is the full width at half maximum intensity of the peak, and θ is the angle for the XRD peak), the crystallite size of the composites has been estimated as approximately 0.2 μm, which is much larger than nanoparticles, therefore, the composites synthesized are not nanoparticles..

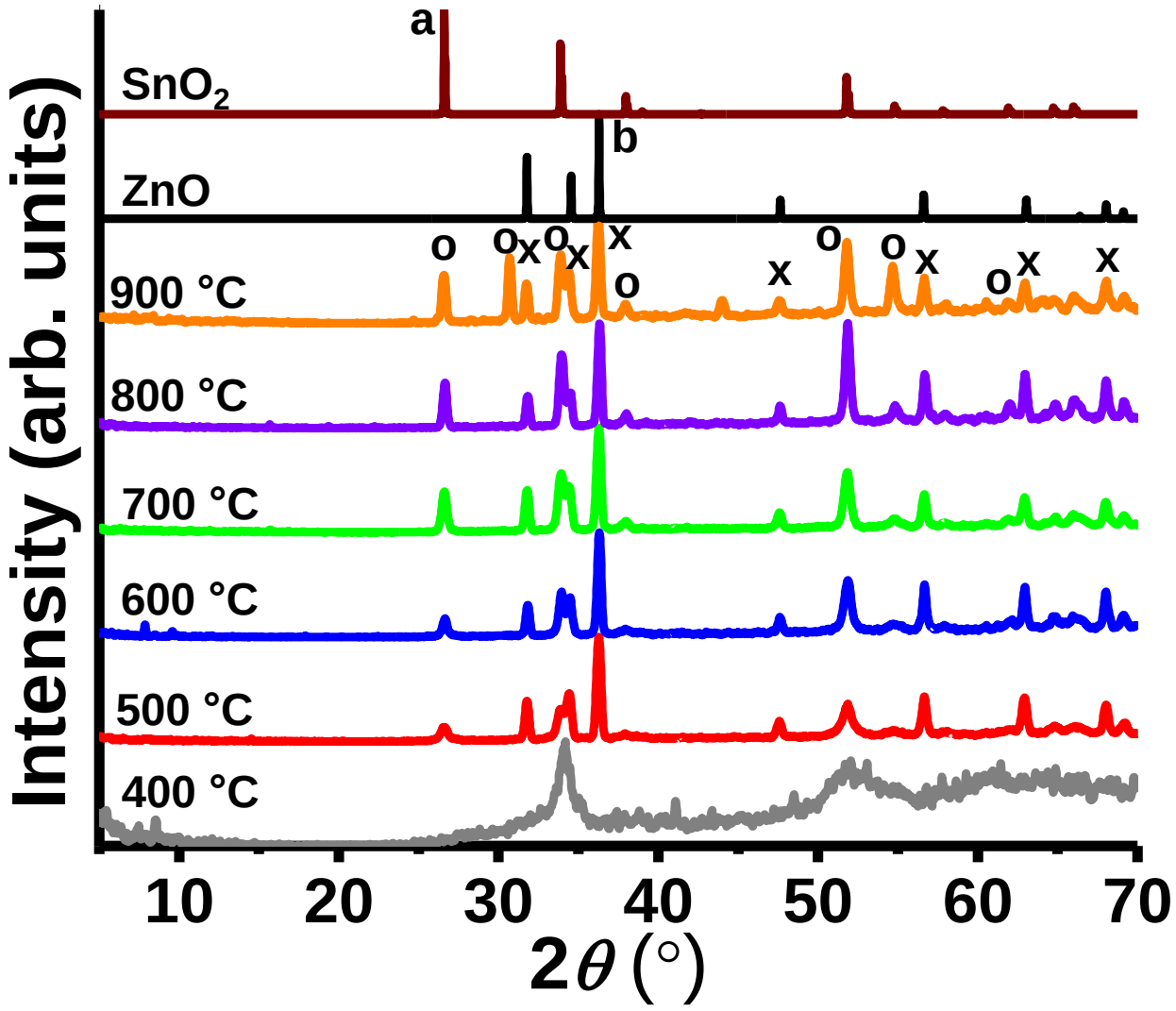

Figure 1 PXRD patterns of the all composites in this work. The ZnO peaks are marked with "x", while the SnO_2 peaks are marked with "o". The composite synthesized at 900 °C has a couple impurity peaks, and elemental analysis showed that it contains a small amount of Ba, so that is likely the origin of those impurity peaks.

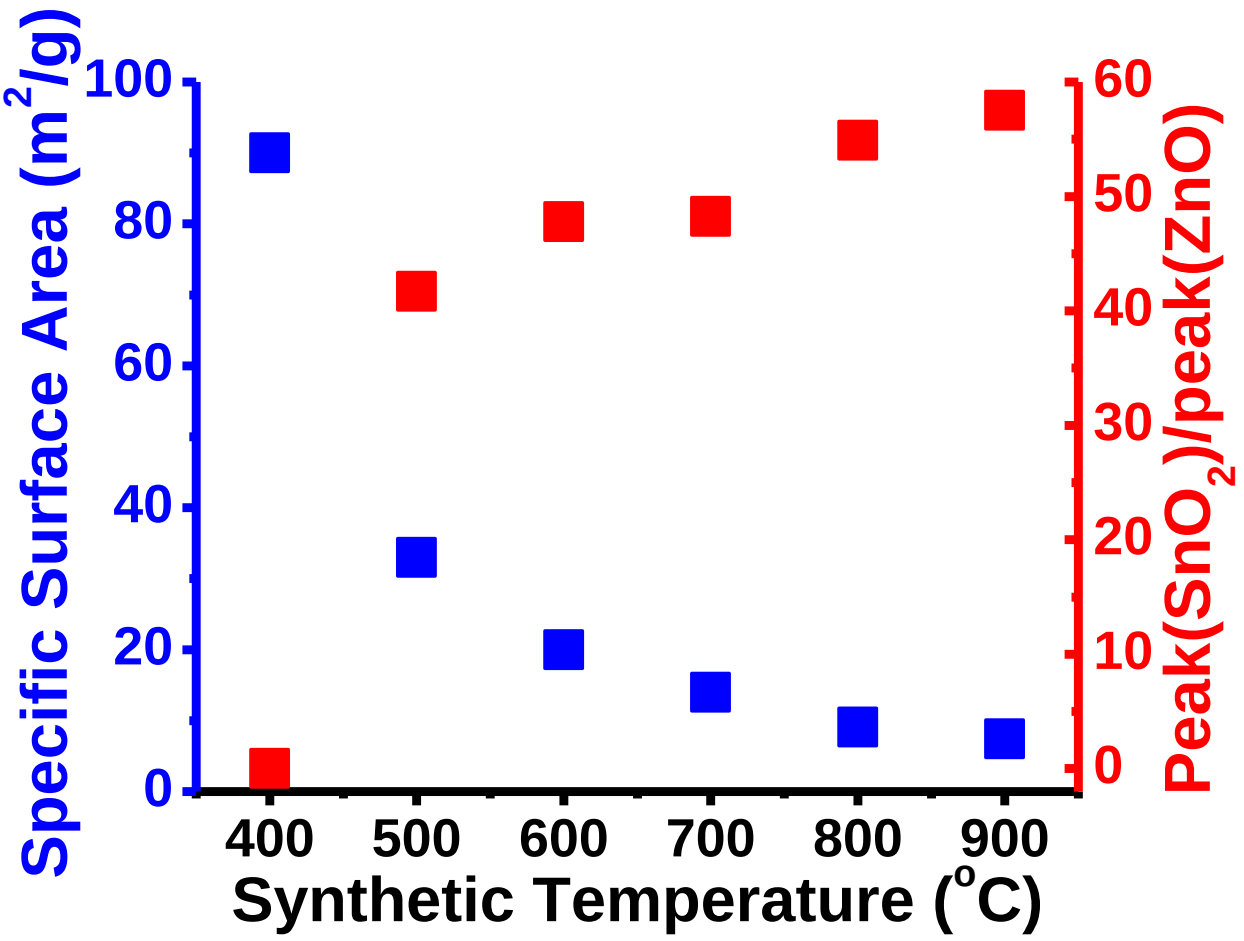

Figure 2 Specific surface area (left axis; blue circles) and crystallinity of SnO_2 (right axis; red triangles) in each composite. Crystallinity is represented by the ratio of the height of the most intense peak of SnO_2 (Peak a in Figure 1) to the height of the most intense peak of ZnO (Peak b in Figure 1). The composited synthesized at 400 °C is amorphous, so its peak height is assumed to be zero.

The specific surface areas of each ZnO-SnO_2 composite are shown in Figure 2 and listed in Table 1. As the synthetic temperature increases, the surface area decreases, likely due to coalescence of solid particles.

Synthetic Temperature (°C)	400	500	600	700	800	900
Specific Surface Area (m^2/g)	90	33	20	14	9.1	7.4
n(ZnO)/n(SnO_2)	0.78	2.77	2.51	2.06	2.34	2.40
Bandgap Energy (eV)	NA	3.30	3.28	3.27	3.29	3.28

Table 1 Specific surface areas, compositions, and bandgap energies of the ZnO-SnO_2 composites synthesized in this work.

The IR spectra of the composites are shown in Figure 3. All composites showed a broad peak in the range of 400-700 cm^{-1}, which corresponds to the Zn-O stretch (457 cm^{-1})[52] in ZnO and the Sn-O stretch in SnO_2 (a series of peaks between 526 cm^{-1} and 690 cm^{-1})[53]. For the composite synthesized at 400 °C, the peak appears to be just one broad peak; while for composites synthesized at 500 °C and above, the peak appears to have separated into two: one is a more intense peak just above 400 cm^{-1}, which likely corresponds to the Zn-O stretch, the other is a shoulder (composites synthesized at 500 °C and 600 °C) or a series of less intense peaks (composites synthesized at 700 °C, 800 °C, and 900 °C) between 570 cm^{-1} and 690 cm^{-1}, which likely corresponds to the Sn-O stretch. That difference in IR spectra of the composites synthesized at different temperatures is likelydue to the increased crystallinity of the composites as the synthetic temperature increased.

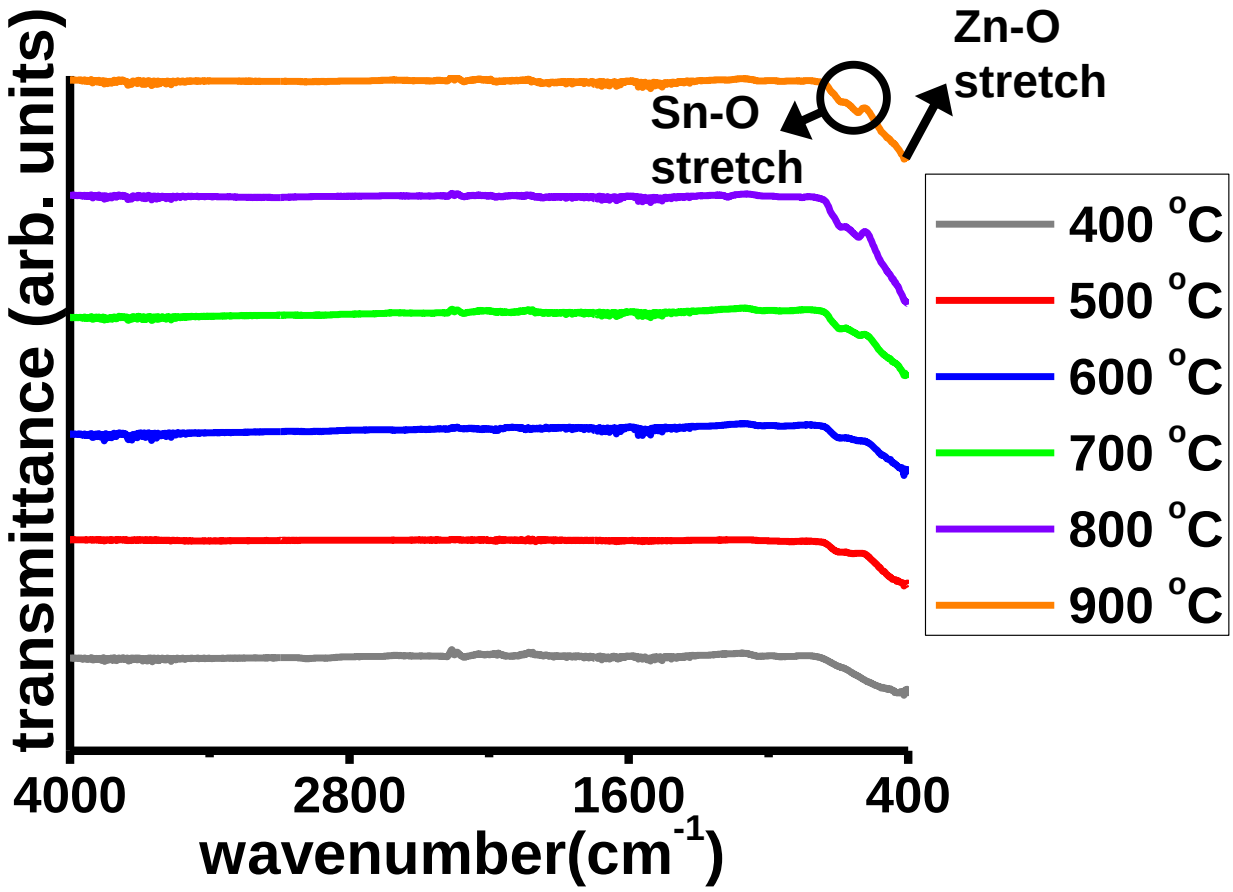

Figure 3 IR spectra of the ZnO-SnO_2 composites in this study. The synthetic temperature of each composite is included in the figure legend. The peaks corresponding to the Zn-O stretch and the Sn-O stretch are indicated in the figure.

The SEM images (Figure 4) of the composites synthesized at 400 °C show particles of different sizes and shapes, while the SEM images of composites synthesized at higher temperatures show coalesced particles. The heterojunctions between ZnO and SnO_2 are not shown in the SEM images, thus from the SEM images alone, it is inconclusive whether the samples synthesized were composites. The elemental analysis (represented as n(ZnO)/n(SnO_2) in Table 1) revealed an average molar ratio of Zn: Sn ≈ 2.4: 1 for composites synthesized at 500 °C and above, consistent with the molar ratio of the starting materials.

The elemental analysis for the composite synthesized at 400 °C, however, revealed a molar ratio of Zn: Sn ≈ 0.78: 1, which indicates that it still contains both ZnO andSnO_2but with less ZnO than the other composites. Since it has been found that $ZnCl_2$ only starts to get partially oxidized to ZnO when the temperature reached 400 °C[54], it is likely because synthetic reaction and crystallization of the composite was incomplete after heating for 24 hours at 400 °C, and when the product was washed with water, the excess $ZnCl_2$ was dissolved and remained in the decantant. The elemental analysis for the composite synthesized at 900 °C aslo revealed a small amount of Ba in the sample, likely due to Ba_2SnO_4 decomposed to BaO at the high temperature, which accounts for the few impurity peaks in the PXRD pattern of that composite.

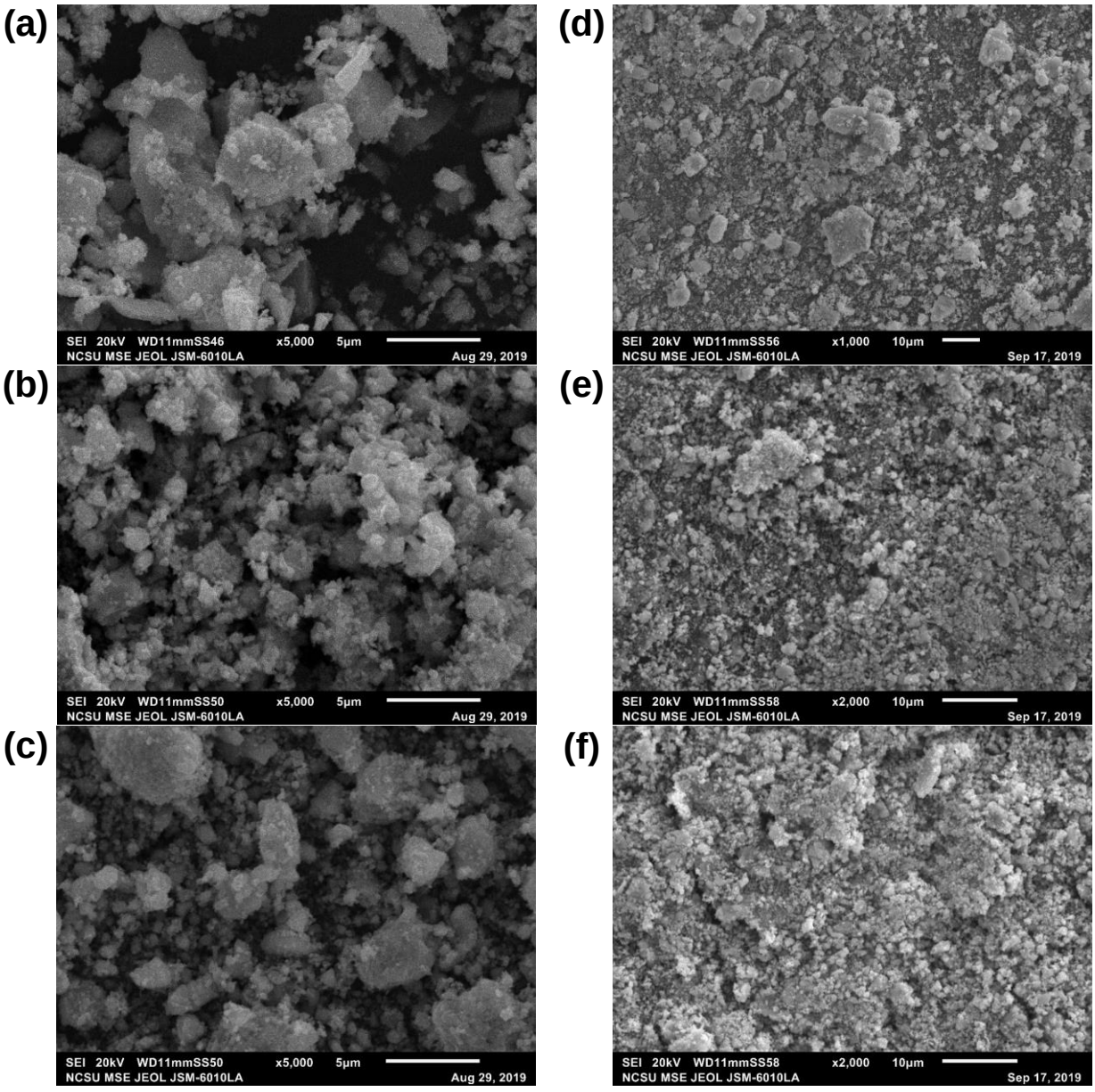

Figure 4 SEM images of the ZnO-SnO_2 composites synthesized at (a) 400 °C, (b) 500 °C, (c) 600 °C, (d) 700 °C, (e) 800 °C, (f) 900 °C.

Optical diffuse reflectance spectra of the ZnO-SnO_2 composites synthesized at 500 °C and above are shown in Figure 5, and their bandgap energies are listed in Table 1. The composite synthesized at 400 °C is amorphous, thus its band gap size was not measured. The bandgap energies are similar for all composites, and are all right outside the visible light region. The bandgap energy of the light yellow colored composite synthesized at 500 °C is not significantly different from those of the white colored composites synthesized at other temperatures, which indicates that its color likely does not come from any differences in their band gap. The bandgap energies for all ZnO-SnO_2 composites are between that of pure ZnO (3.17 eV) and that of pure SnO_2 (3.55 eV),[35] which also indicates that the materials synthesized contain both ZnO and SnO_2.

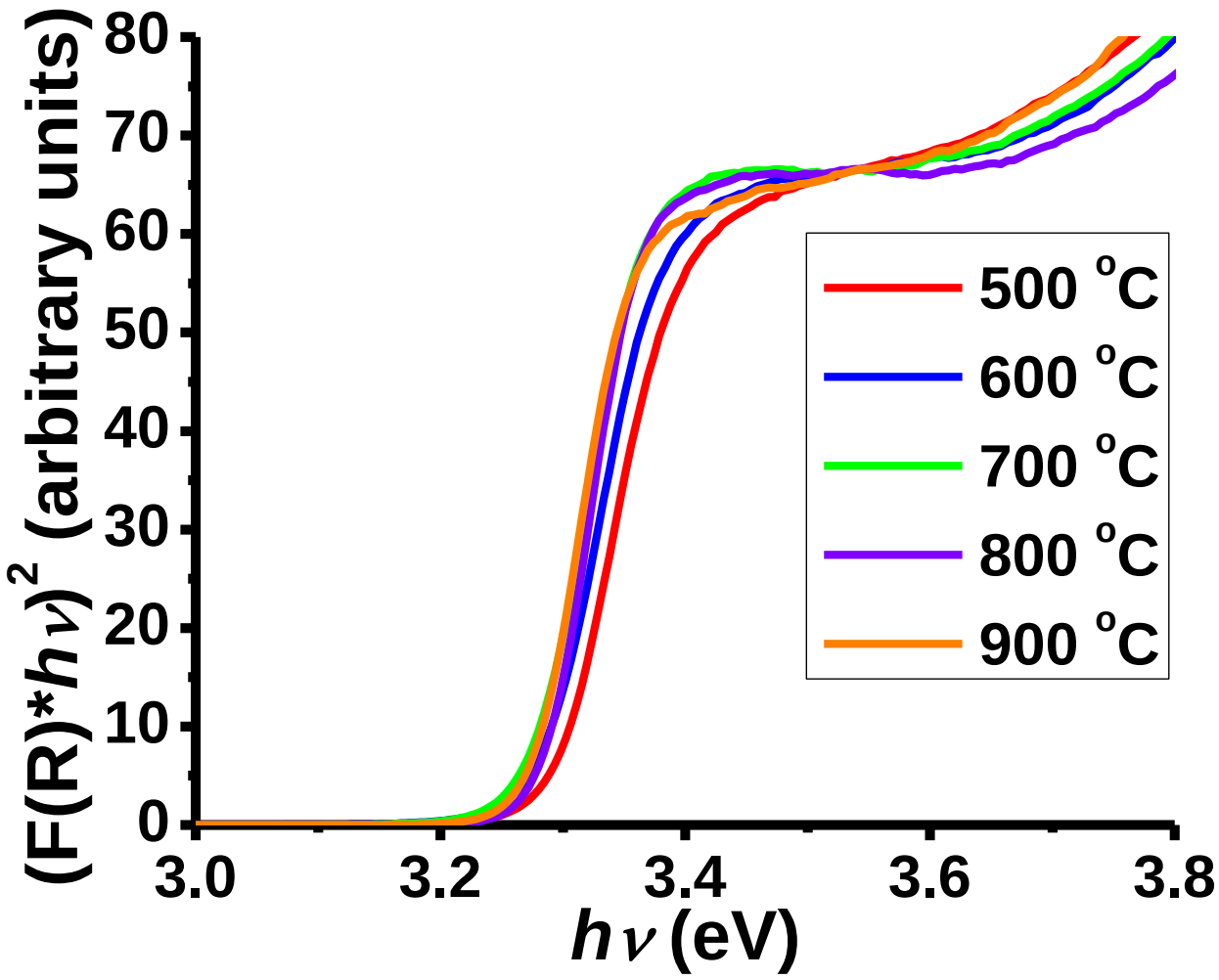

Figure 5 UV-Vis Diffuse Reflectance Spectra for bandgap energymeasurements of composites synthesized at 500 °C and above.

3.2 Photocatalytic Activities

The photocatalytic activity of each ZnO-SnO_2 composite was investigated for the degradation of the organic dye, methylene blue (MB). During each photocatalytic MB degradation reaction and each control reaction, the concentration of MB in the solution was monitored by UV-Vis spectra, and the results are shown in Figure S2. For each experiment, at each time point, the concentration of MB in the solution is

represented by the height of the absorbance peak, which was calculated as the difference between the bottom of the peak (calculated as an average of the beginning and the end of the peak if the baseline is not flat) and the maximum of the peak. The heights of the absorbance peaks during the reaction were each divided by the height of the absorbance peak at the beginning of the reaction to obtain the change of concentration relative to the initial concentration (C/C_0), and then plotted against time. The results are shown in Figure 6(a) and 6(b). After each photocatalytic dye degradation experiment, PXRD pattern was obtained on the composite used as the photocatalyst, and as shown in Figure S1, the structure of the composite did not change before and after the photocatalytic dye degradation experiment, which indicates that no chemical changes have occurred to the composites, consistent with their role as catalysts. To verify that the ZnO-SnO_2 composites synthesized are indeed composites instead of simple phase mixtures of ZnO and SnO_2, pure ZnO, pure SnO_2, and a mixture of commercial ZnO and SnO_2 (at a molar ratio of 2.5:1, similar to that in the ZnO-SnO_2 composites in this study) were each heated to 500 °C for 24 h under the same procedure as in the syntheses of the composites in this study, and the same photocatalytic degradation of MB were performed with MB solution of the same concentration mixed with each of them. The results are included in Figure 6(a) and 6(b). Also, since the synthetic procedure was initially designed to synthesize Zn_2SnO_4, the same photocatalytic degradation of MB was performed on pure Zn_2SnO_4, synthesized using a hydrothermal method, and the result was also included in Figure 6(a) and 6(b).

For a better comparison of the photocatalytic activities of composites synthesized at different temperatures, pure ZnO, pure SnO_2, pure Zn_2SnO_4, and the simple phase mixture of ZnO and SnO_2 as mentioned above, kinetic analysis was performed on the photocatalytic degradation of MB to obtain the rate constants. Photocatalytic degradation of MB has been found to follow a pseudo-first order mechanism[15,20,29,55,56]:

$$C = C_0 e^{-kt} \text{ or } \ln\frac{C}{C_0} = -kt \qquad \text{(Equation 1)}$$

where C_0 is the initial concentration of MB, C is the concentration of MB at time t, and k is the rate constant of the photocatalytic MB degradation reaction. According to Beer-Lambert's law, the absorption is directly proportional to the concentration, so the absorptions of MB during the degradation reactions were used in place of concentrations in Equation 1 to find the rate constants. The rate constants of the photocatalytic MB degradation reaction catalyzed by each of the composites in this study, as well as for pure ZnO, pure SnO_2, pure Zn_2SnO_4, and the simple phase mixture of ZnO and SnO_2 as mentioned above were determined using Equation 1, and the results were included in Figure 6(b).

As shown in Figures 6(a) and 6(b), The ZnO-SnO_2 composite synthesized at 400 °C showed much lower photocatalytic activity compared to composites synthesized at higher temperatures. The photocatalytic activity showed a slight decrease between the ZnO-SnO_2 composite synthesized at 500 °C and that synthesized at 600 °C, then increases from the composite at 600 °C to the composite synthesized at 900 °C. All composites synthesized in this study show high photocatalytic activities, especially the composites synthesized at 500 °C and above: when catalyzed by those composites, the concentration of the dye decreased to 10% or less of the original concentration after approximately 10 minutes, and completely degraded after 20 minutes. The rate constants of the MB degradation reactions catalyzed by the composites in this study are all comparable or higher than reported for ZnO-SnO_2 composites in literature[15,20,29,55,56]. The rate constant of the MB degradation reactions catalyzed by ZnO is much higher than catalyzed by SnO_2, and the rate constant of the reaction catalyzed by the 2.5: 1 mixture of ZnO and SnO_2 is in between those two, which is consistent with it being a simple phase mixture of ZnO and SnO_2. By contrast, the rate constants of the MB degradation reactions catalyzed by composites synthesized at 500 °C and above are all comparable or higher than the rate constants of the reaction catalyzed by pure

ZnO, pure SnO_2, pure Zn_2SnO_4, and the simple phase mixture of ZnO and SnO_2 at 2.5 to 1 molar ratio, which indicates higher photocatalytic activities for those composites, and thus they are likely composites instead of simple mixtures of ZnO and SnO_2.

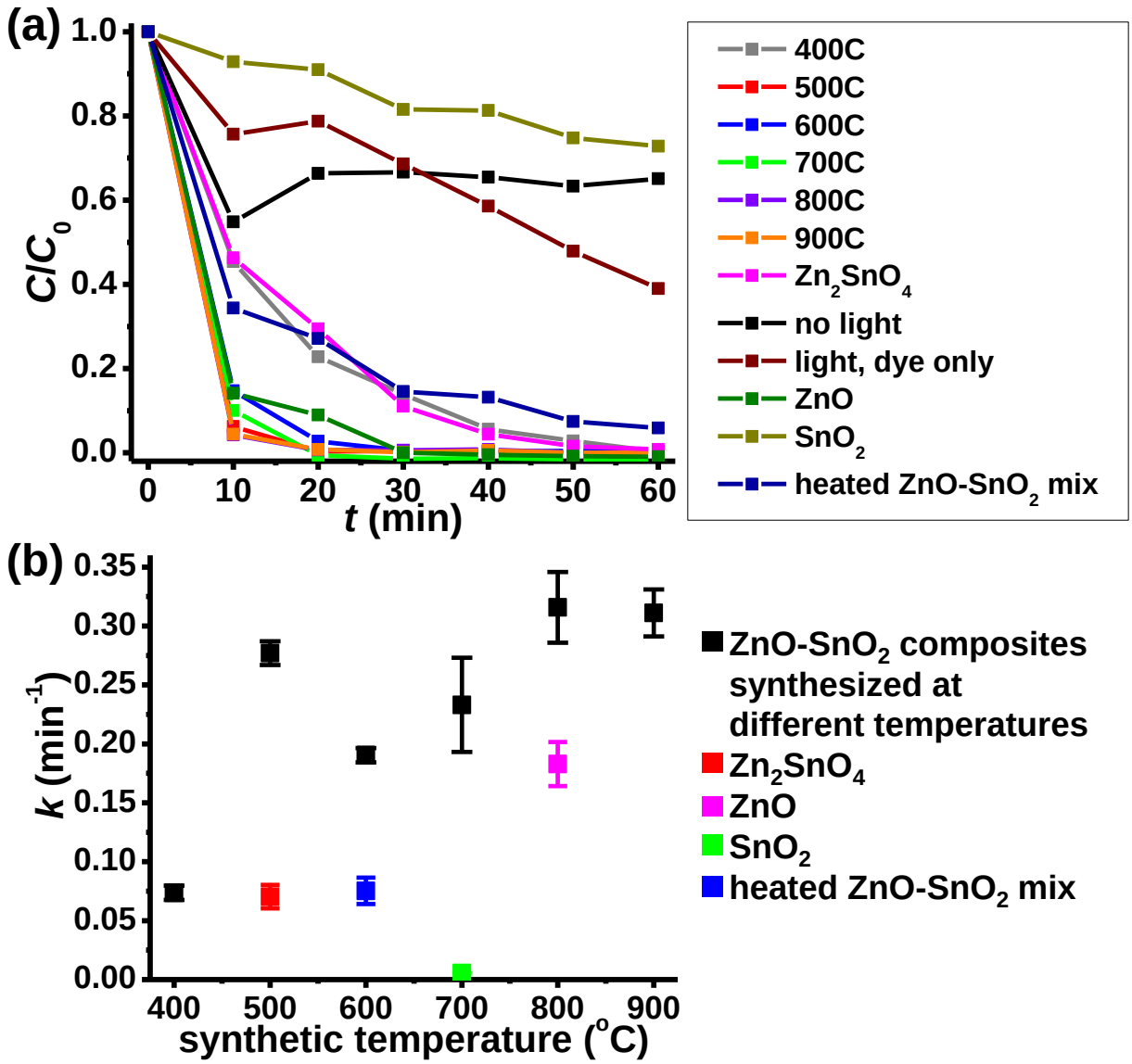

Figure 6 (a) Photocatalytic degradation of MB in aqueous solution (initial concentration: 1.0×10^{-5} *M*) with each ZnO-SnO_2 composite (30 mg composite in 35 mL MB solution, or 0.857 g composite/1 L MB solution) synthesized at different temperatures, represented as the ratio of the concentration of the remaining dye to the original concentration of the dye with time, monitored by UV-Vis spectra. The results of the control experiments are also shown in the figure. (b) The rate constants (with error bars) of each photocatalytic dye degradation reaction mixed with different solids. The rate constants of the photocatalytic dye degradation reactions catalyzed by the samples synthesized at different temperatures were represented by the black squares, and the rate constants of photocatalytic dye degradation reactions mixed with pure ZnO heated at 500 °C for 24 hours (magenta), pure SnO_2 heated at 500 °C for 24 hours

(green), pure Zn_2SnO_4 (red), and a simple mixture of ZnO and SnO_2 at 2.5: 1 molar ratio heated at 500 °C for 24 hours (blue), were also included in the figure (placed at arbitrary synthetic temperatures) for comparison.

During the photocatalytic degradation of MB in water, the compounds absorb photons with energies greater than their bandgap energies, which leads to electron transfer from the valence band to the conduction band, creating positive holes in the valence band. The holes can then directly oxidize the carboxylic acid groups in MB and resulting in its degradation.[7] With the bandgap energies around 3.17 eV and 3.55 eV, respectively, the electrons in ZnO and SnO_2 can be excited by light of wavelengths 391 nm and 349 nm, respectively, both of which are in the UV region.[35] Since the bandgap energies of the ZnO-SnO_2 samples are around 3.30 eV, their photocatalytic activities likely come from excitation by the UV light from the lamp. Under light irradiation, electrons are excited from the valence band into the conduction band, leaving positive holes in the valence band, and both the holes and the excited electrons will lead to the formation of •OH and O_2^- radicals, which further leads to the degradation of the dye.[7,15,18,19,27-29] Therefore, materials with high photocatalytic activities must be able to absorb the energy of the light irradiation and generate excited electrons and holes, and the photogenerated electrons and holes must have long enough lifetime for them to generate the radicals. It has been found that the conduction band of SnO_2 is lower than that of ZnO, so that it can act as the sink for the photogenerated electrons from ZnO; moreover, at the heterojunction between ZnO and SnO_2, the photogenerated positive holes in the valence band of SnO_2 can move to the valence band of ZnO, which leads to more efficient charge separation and less electron-hole recombination, and results in increased photocatalytic activities in ZnO-SnO_2 composites compared to pure ZnO or pure SnO_2 in which fast electron-hole recombination hinders their photocatalytic activity (Figure 7).[11,14,17-19,26,28,29,35] Since rate constants (and thus photocatalytic activities) of photocatalytic MB degradation reaction catalyzed by composites synthesized at 500 °C and above are higher than the reaction catalyzed by the simple phase mixture of ZnO and SnO_2 at similar molar ratio, the ZnO-SnO_2 composites synthesized at 500 °C and above are likely composites with heterojunctions between ZnO and SnO_2, instead of simple phase mixtures of ZnO and SnO_2.

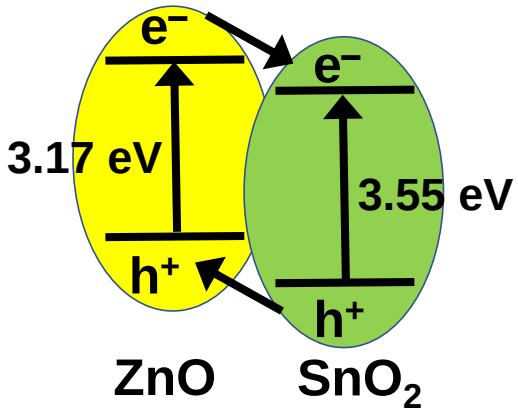

Figure 7 Schematic representation of the band gaps of ZnO-SnO_2 composites.

From the results, it is likely that the photocatalytic activities of the composites are affected by both their specific surface areas and their compositions and crystallinities. As the synthetic temperature

increases, the surface area of the composites decreases (Figure 2), which leads to decreased photocatalytic activity due to fewer sites to adsorb the dye molecules. By contrast, as the synthetic temperature increases, the crystallinity increases (Figure 2), which leads to increased photocatalytic activity due to smaller concentration of defects in the sample and thus higher mobility of the excited carriers (excited electrons and/or holes)[57,58], as has also been shown in literature for other photocatalysts[59-63]. For the ZnO-SnO_2 composite synthesized at 400 °C, although it has the highest specific surface area to adsorb the dye, it is also amorphous and has a lower ZnO percentage likely due to the synthesis reaction being incomplete at such low temperature. An amorphous solid has significantly more defects than a crystalline solid due to its lack of long-range order, and thus the mobility of excited carriers are impeded[5757,58]. Meanwhile, a lower ZnO percentage leads to fewer ZnO-SnO_2 heterojunction, which is critical for improved photocatalytic activity of ZnO-SnO_2 composite, as discussed in the previous paragraph. Those two factors likely accounts for its photocatalytic activity being the lowest among all composites. The composite synthesized at 500 °C and above have similar compositions (ZnO: $SnO_2 \approx 2.4$ on average) thus likely similar number of ZnO-SnO_2 heterojunctions. The composite synthesized at 500 °C has a larger specific surface area than composites synthesized at higher temperatures, but it also has the lowest crystallinity, which partially negates the increase in its photocatalytic activity due to its large surface area, thus the composite synthesized at 500 °C has only a slightly higher photocatalytic activity than those synthesized at 600 °C and 700 °C and comparable photocatalytic activity as those synthesized at 800 °C and 900 °C, despite its surface area being much higher. For composites synthesized at 600 °C and above, even though the surface area decreases as the temperature of the synthesis increases, the crystallinity of the composite increases, which leads to higher mobility of the excited carriers, and thus their photocatalytic activities increase. Therefore, an interplay of the surface areas and crystallinities of the composites resulted in the non-monotonically varied photocatalytic activity of the composites with their synthetic temperatures,

For comparison, the same experimental procedure for the photocatalytic degradation of MB was performed on MB solution of the same concentration under light irradiation without any catalyst, and MB solution of the same concentration with the ZnO-SnO_2 composite synthesized at 500 °C without light irradiation. The results are also shown in Figure 5. Without any catalyst, MB showed much less degradation under light irradiation. With the ZnO-SnO_2 composite but without light irradiation, the concentration of MB in the solution decreased at the beginning of the experiment, likely due to the adsorption of MB onto the solid particles of the composite; after that, the concentration of MB in the solution remained the same. Those comparison experiments confirmed that the composites catalyzed the degradation of MB under light irradiation.

Since both the surface area and the crystallinity of the composite can be changed by using different temperatures in the flux synthesis, as indicated in Table 1 and Figure 2, the flux synthetic approach provides a possible way to tune and maximize the photocatalytic activity of ZnO-SnO_2 composites: to maximize the photocatalytic activity of the ZnO-SnO_2 composite, a moderate temperature should be used in the flux synthesis to obtain a ZnO-SnO_2 composite with relatively high crystallinity without the surface area getting too low.

4. Conclusion

ZnO-SnO_2 composites were synthesized using the molten-salt flux mediated method at temperatures ranging from 400 °C to 900 °C. Each synthesis was accomplished by reacting molten $ZnCl_2$ reacted with Ba_2SnO_4, with $ZnCl_2$ being both the flux and one of the reactants. The crystallinity of the composites increases as the synthetic temperatures increases, with the composite synthesized at 400 °C being amorphous and also having the lowest percentage of ZnO in the composite. The specific surface areas of

the composites decrease with increasing synthetic temperatures. Under UV-Visible light irradiation, the composites all demonstrated photocatalytic activities for the degradation of methylene blue, with the color of the dye disappeared mostly within 10 minutes, and completely within 20 minutes using composites synthesized at 500 °C and above. Photocatalytic activities of composites synthesized at 500 °C and above are all higher than that of a simple phase mixture of ZnO and SnO_2, which indicates that they are likely composites with ZnO-SnO_2 heterojunctions that enhanced their photocatalytic activities, instead of simple mixtures of ZnO and SnO_2. Their photocatalytic activities increase as their crystallinity increases and as the percentage of ZnO in the composite increases, which is likely due to higher mobility of excited carriers as well as increased ZnO-SnO_2 heterojunctions; and their photocatalytic activities decrease as their specific surface areas decrease, which is likely due to the decreased active sites on the surface to adsorb methylene blue molecules. Therefore, an interplay between the crystallinity and the surface areas of the composites leads to their varied photocatalytic activities.

This study introduced a new approach to synthesize ZnO-SnO_2 composites with high photocatalytic activities for the degradation of organic dyes, and provided insights into factors that affect their photocatalytic activities. Furthermore, since both crystallinity and surface areas of the composite change with the temperature of the synthesis, the molten-salt flux mediated synthetic approach proposed here provides a possible way to maximize the photocatalytic activity of the composite by changing the temperature of the synthesis alone to produce ZnO-SnO_2 composites with relatively high crystallinity and surface area.

Acknowledgements

The authors acknowledge Dr. Paul Maggard from North Carolina State University for his generosity of letting us use his lab equipment and valuable personal discussions on this work.

References

(1) Kumar, P. S.; Saravanan, A. In *Sustainable fibres and textiles*; Elsevier: 2017, p 323-346.

(2) Ali, M. B.; Barras, A.; Addad, A.; Sieber, B.; Elhouichet, H.; Férid, M.; Szunerits, S.; Boukherroub, R. Co 2 SnO 4 nanoparticles as a high performance catalyst for oxidative degradation of rhodamine B dye and pentachlorophenol by activation of peroxymonosulfate. *PCCP* **2017**, *19*, 6569-6578.

(3) Feng, Y.-N.; Wang, H.-C.; Luo, Y.-D.; Shen, Y.; Lin, Y.-H. Ferromagnetic and photocatalytic behaviors observed in Ca-doped BiFeO3 nanofibres. *J. Appl. Phys.* **2013**, *113*, 146101.

(4) Han, F.; Kambala, V. S. R.; Srinivasan, M.; Rajarathnam, D.; Naidu, R. Tailored titanium dioxide photocatalysts for the degradation of organic dyes in wastewater treatment: a review. *Applied Catalysis A: General* **2009**, *359*, 25-40.

(5) Wang, W.; Tadé, M. O.; Shao, Z. Research progress of perovskite materials in photocatalysis-and photovoltaics-related energy conversion and environmental treatment. *Chem. Soc. Rev.* **2015**, *44*, 5371-5408.

(6) Wu, J.; Huang, F.; Lü, X.; Chen, P.; Wan, D.; Xu, F. Improved visible-light photocatalysis of nano-Bi 2 Sn 2 O 7 with dispersed s-bands. *J. Mater. Chem.* **2011**, *21*, 3872-3876.

(7) Houas, A.; Lachheb, H.; Ksibi, M.; Elaloui, E.; Guillard, C.; Herrmann, J.-M. Photocatalytic degradation pathway of methylene blue in water. *Appl. Catal., B* **2001**, *31*, 145-157.

(8) Zarepour, M. A.; Tasviri, M. Facile fabrication of Ag decorated TiO2 nanorices: Highly efficient visible-light-responsive photocatalyst in degradation of contaminants. *Journal of Photochemistry and Photobiology A: Chemistry* **2019**, *371*, 166-172.

(9) Fazlali, F.; Hajian, A.; Afkhami, A.; Bagheri, H. A superficial approach for fabricating unique ternary AgI@ TiO2/Zr-MOF composites: An excellent interfacial with improved photocatalytic light-responsive under visible light. *Journal of Photochemistry and Photobiology A: Chemistry* **2020**, 112717.

(10) Fang, X.; Lu, G.; Mahmood, A.; Tang, Z.; Liu, Z.; Zhang, L.; Wang, Y.; Sun, J. A Novel Ternary Mica/TiO2/Fe2O3 Composite Pearlescent Pigment for the Photocatalytic Degradation of Gaseous Acetaldehyde. *Journal of Photochemistry and Photobiology A: Chemistry* **2020**, 112617.

(11) Cun, W.; Jincai, Z.; Xinming, W.; Bixian, M.; Guoying, S.; Ping'an, P.; Jiamo, F. Preparation, characterization and photocatalytic activity of nano-sized ZnO/SnO2 coupled photocatalysts. *Applied Catalysis B: Environmental* **2002**, *39*, 269-279.

(12) Wang, C.; Wang, X.; Xu, B.-Q.; Zhao, J.; Mai, B.; Sheng, G.; Fu, J. Enhanced photocatalytic performance of nanosized coupled ZnO/SnO2 photocatalysts for methyl orange degradation. *Journal of Photochemistry and Photobiology A: Chemistry* **2004**, *168*, 47-52.

(13) Wang, W. W.; Zhu, Y. J.; Yang, L. X. ZnO–SnO2 hollow spheres and hierarchical nanosheets: hydrothermal preparation, formation mechanism, and photocatalytic properties. *Adv. Funct. Mater.* **2007**, *17*, 59-64.

(14) Zhang, M.; An, T.; Hu, X.; Wang, C.; Sheng, G.; Fu, J. Preparation and photocatalytic properties of a nanometer ZnO–SnO2 coupled oxide. *Applied Catalysis A: General* **2004**, *260*, 215-222.

(15) Zhang, Z.; Shao, C.; Li, X.; Zhang, L.; Xue, H.; Wang, C.; Liu, Y. Electrospun nanofibers of ZnO− SnO2 heterojunction with high photocatalytic activity. *The Journal of Physical Chemistry C* **2010**, *114*, 7920-7925.

(16) Zhang, M.; Sheng, G.; Fu, J.; An, T.; Wang, X.; Hu, X. Novel preparation of nanosized ZnO–SnO2 with high photocatalytic activity by homogeneous co-precipitation method. *Mater. Lett.* **2005**, *59*, 3641-3644.

(17) Hamrouni, A.; Lachheb, H.; Houas, A. Synthesis, characterization and photocatalytic activity of ZnO-SnO2 nanocomposites. *Materials Science and Engineering: B* **2013**, *178*, 1371-1379.

(18) Seftel, E.; Popovici, E.; Mertens, M.; Stefaniak, E.; Van Grieken, R.; Cool, P.; Vansant, E. SnIV-containing layered double hydroxides as precursors for nano-sized ZnO/SnO2 photocatalysts. *Applied Catalysis B: Environmental* **2008**, *84*, 699-705.

(19) Liu, R.; Huang, Y.; Xiao, A.; Liu, H. Preparation and photocatalytic property of mesoporous ZnO/SnO2 composite nanofibers. *J. Alloys Compd.* **2010**, *503*, 103-110.

(20) Martínez, D. T.; Pérez, R. C.; Delgado, G. T.; Ángel, O. Z. Structural, morphological, optical and photocatalytic characterization of ZnO–SnO2 thin films prepared by the sol–gel technique. *Journal of Photochemistry and Photobiology A: Chemistry* **2012**, *235*, 49-55.

(21) Wang, Z.; Li, Z.; Zhang, H.; Wang, C. Improved photocatalytic activity of mesoporous ZnO–SnO2 coupled nanofibers. *Catal. Commun.* **2009**, *11*, 257-260.

(22) Yang, Z.; Lv, L.; Dai, Y.; Xv, Z.; Qian, D. Synthesis of ZnO–SnO2 composite oxides by CTAB-assisted co-precipitation and photocatalytic properties. *Appl. Surf. Sci.* **2010**, *256*, 2898-2902.

(23) Kowsari, E.; Ghezelbash, M. R. Ionic liquid-assisted, facile synthesis of ZnO/SnO2 nanocomposites, and investigation of their photocatalytic activity. *Mater. Lett.* **2012**, *68*, 17-20.

(24) Ghaderi, A.; Abbasi, S.; Farahbod, F. Synthesis of SnO2 and ZnO nanoparticles and SnO2-ZnO hybrid for the photocatalytic oxidation of methyl orange. *Iranian Journal of Chemical Engineering (IJChE)* **2015**, *12*, 96-105.

(25) Pascariu, P.; Airinei, A.; Olaru, N.; Olaru, L.; Nica, V. Photocatalytic degradation of Rhodamine B dye using ZnO–SnO2 electrospun ceramic nanofibers. *Ceram. Int.* **2016**, *42*, 6775-6781.

(26) Lin, J.; Luo, Z.; Liu, J.; Li, P. Photocatalytic degradation of methylene blue in aqueous solution by using ZnO-SnO2 nanocomposites. *Mater. Sci. Semicond. Process.* **2018**, *87*, 24-31.

(27) Lin, C.-C.; Chiang, Y.-J. Feasibility of using a rotating packed bed in preparing coupled ZnO/SnO2 photocatalysts. *Journal of Industrial and Engineering Chemistry* **2012**, *18*, 1233-1236.

(28) Zheng, L.; Zheng, Y.; Chen, C.; Zhan, Y.; Lin, X.; Zheng, Q.; Wei, K.; Zhu, J. Network structured SnO2/ZnO heterojunction nanocatalyst with high photocatalytic activity. *Inorg. Chem.* **2009**, *48*, 1819-1825.

(29) Uddin, M. T.; Nicolas, Y.; Olivier, C.; Toupance, T.; Servant, L.; Müller, M. M.; Kleebe, H.-J.; Ziegler, J. r.; Jaegermann, W. Nanostructured SnO2–ZnO heterojunction photocatalysts showing enhanced photocatalytic activity for the degradation of organic dyes. *Inorg. Chem.* **2012**, *51*, 7764-7773.

(30) Verma, N.; Yadav, S.; Marí, B.; Mittal, A.; Jindal, J. Synthesis and charcterization of coupled ZnO/SnO2 photocatalysts and their activity towards degradation of cibacron red dye. *Transactions of the Indian Ceramic Society* **2018**, *77*, 1-7.

(31) Ali, W.; Ullah, H.; Zada, A.; Alamgir, M. K.; Muhammad, W.; Ahmad, M. J.; Nadhman, A. Effect of calcination temperature on the photoactivities of ZnO/SnO2 nanocomposites for the degradation of methyl orange. *Mater. Chem. Phys.* **2018**, *213*, 259-266.

(32) Dong, S.; Cui, L.; Tian, Y.; Xia, L.; Wu, Y.; Yu, J.; Bagley, D. M.; Sun, J.; Fan, M. A novel and high-performance double Z-scheme photocatalyst ZnO-SnO2-Zn2SnO4 for effective removal of the biological toxicity of antibiotics. *J. Hazard. Mater.* **2020**, 123017.

(33) Sakthivel, S.; Neppolian, B.; Shankar, M.; Arabindoo, B.; Palanichamy, M.; Murugesan, V. Solar photocatalytic degradation of azo dye: comparison of photocatalytic efficiency of ZnO and TiO2. *Sol. Energy Mater. Sol. Cells* **2003**, *77*, 65-82.

(34) Lamba, R.; Umar, A.; Mehta, S.; Kansal, S. K. Well-crystalline porous ZnO–SnO2 nanosheets: an effective visible-light driven photocatalyst and highly sensitive smart sensor material. *Talanta* **2015**, *131*, 490-498.

(35) Hamrouni, A.; Moussa, N.; Parrino, F.; Di Paola, A.; Houas, A.; Palmisano, L. Sol–gel synthesis and photocatalytic activity of ZnO–SnO2 nanocomposites. *J. Mol. Catal. A: Chem.* **2014**, *390*, 133-141.

(36) Elwell, D.; Neate, B. Mechanisms of crystal growth from fluxed melts. *Journal of Materials Science* **1971**, *6*, 1499-1519.

(37) Liu, X.; Fechler, N.; Antonietti, M. Salt melt synthesis of ceramics, semiconductors and carbon nanostructures. *Chem. Soc. Rev.* **2013**, *42*, 8237-8265.

(38) Noureldine, D.; Anjum, D. H.; Takanabe, K. Flux-assisted synthesis of SnNb 2 O 6 for tuning photocatalytic properties. *PCCP* **2014**, *16*, 10762-10769.

(39) Arney, D.; Hardy, C.; Greve, B.; Maggard, P. A. Flux synthesis of AgNbO3: effect of particle surfaces and sizes on photocatalytic activity. *Journal of Photochemistry and Photobiology A: Chemistry* **2010**, *214*, 54-60.

(40) Yoshida, H.; Yamamoto, A. In *AIP Conference Proceedings*; AIP Publishing LLC: 2016; Vol. 1729, p 020001.

(41) Shivakumara, C. Low temperature synthesis and characterization of rare earth orthoferrites LnFeO3 (Ln= La, Pr and Nd) from molten NaOH flux. *Solid State Commun.* **2006**, *139*, 165-169.

(42) Hamilton, A. M.; O'Donnell, S.; Zoellner, B.; Sullivan, I.; Maggard, P. A. Flux‐mediated synthesis and photocatalytic activity of NaNbO3 particles. *J. Am. Ceram. Soc.* **2020**, *103*, 454-464.

(43) Boltersdorf, J.; King, N.; Maggard, P. A. Flux-mediated crystal growth of metal oxides: synthetic tunability of particle morphologies, sizes, and surface features for photocatalysis research. *CrystEngComm* **2015**, *17*, 2225-2241.

(44) Kennedy, B. J. Neutron powder diffraction study of Sr2SnO4 and Ba2SnO4. *Aust. J. Chem.* **1997**, *50*, 917-920.

(45) Kortüm, G. *Reflectance spectroscopy. Principles, methods, applications*; Springer: Berlin, Heidelberg, New York,, 1969.

(46) Morales, A. E.; Mora, E. S.; Pal, U. Use of diffuse reflectance spectroscopy for optical characterization of un-supported nanostructures. *Revista mexicana de física* **2007**, *53*, 18-22.

(47) Lou, X.; Jia, X.; Xu, J.; Liu, S.; Gao, Q. Hydrothermal synthesis, characterization and photocatalytic properties of Zn2SnO4 nanocrystal. *Materials Science and Engineering: A* **2006**, *432*, 221-225.

(48) Sowa, H.; Ahsbahs, H. High-pressure X-ray investigation of zincite ZnO single crystals using diamond anvils with an improved shape. *J. Appl. Crystallogr.* **2006**, *39*, 169-175.

(49) Elliot, A. D. Structure of pyrrhotite 5C (Fe9S10). *Acta Crystallogr. Sect. B: Struct. Sci.* **2010**, *66*, 271-279.

(50) Rahman, F. Zinc oxide light-emitting diodes: a review. *Optical Engineering* **2019**, *58*, 010901.

(51) Patterson, A. The Scherrer formula for X-ray particle size determination. *Physical review* **1939**, *56*, 978.

(52) Babu, K. S.; Reddy, A. R.; Sujatha, C.; Reddy, K. V.; Mallika, A. Synthesis and optical characterization of porous ZnO. *Journal of Advanced Ceramics* **2013**, *2*, 260-265.

(53) Amalric-Popescu, D.; Bozon-Verduraz, F. Infrared studies on SnO2 and Pd/SnO2. *Catal. Today* **2001**, *70*, 139-154.

(54) Jones, F.; Tran, H.; Lindberg, D.; Zhao, L.; Hupa, M. Thermal stability of zinc compounds. *Energy & fuels* **2013**, *27*, 5663-5669.

(55) Chiang, Y.-J.; Lin, C.-C. Photocatalytic decolorization of methylene blue in aqueous solutions using coupled ZnO/SnO2 photocatalysts. *Powder Technol.* **2013**, *246*, 137-143.

(56) Lin, C.-C.; Chiang, Y.-J. Preparation of coupled ZnO/SnO2 photocatalysts using a rotating packed bed. *Chem. Eng. J.* **2012**, *181*, 196-205.

(57) Hayashi, T.; Hashimoto, Y.; Katsumoto, S.; Iye, Y. Effect of low-temperature annealing on transport and magnetism of diluted magnetic semiconductor (Ga, Mn) As. *Appl. Phys. Lett.* **2001**, *78*, 1691-1693.

(58) Bahl, S.; Chopra, K. Amorphous versus crystalline GeTe films. III. Electrical properties and band structure. *J. Appl. Phys.* **1970**, *41*, 2196-2212.

(59) Kim, D. S.; Kwak, S.-Y. The hydrothermal synthesis of mesoporous TiO2 with high crystallinity, thermal stability, large surface area, and enhanced photocatalytic activity. *Applied Catalysis A: General* **2007**, *323*, 110-118.

(60) Li, Y.-Y.; Zhou, B.-X.; Zhang, H.-W.; Ma, S.-F.; Huang, W.-Q.; Peng, W.; Hu, W.; Huang, G.-F. Doping-induced enhancement of crystallinity in polymeric carbon nitride nanosheets to improve their visible-light photocatalytic activity. *Nanoscale* **2019**, *11*, 6876-6885.

(61) Inagaki, M.; Nonaka, R.; Tryba, B.; Morawski, A. W. Dependence of photocatalytic activity of anatase powders on their crystallinity. *Chemosphere* **2006**, *64*, 437-445.

(62) Shen, H.; Hu, H.; Liang, D.; Meng, H.; Li, P.; Tang, W.; Cui, C. Effect of calcination temperature on the microstructure, crystallinity and photocatalytic activity of TiO2 hollow spheres. *J. Alloys Compd.* **2012**, *542*, 32-36.

(63) Bellardita, M.; Di Paola, A.; Megna, B.; Palmisano, L. Absolute crystallinity and photocatalytic activity of brookite TiO2 samples. *Applied Catalysis B: Environmental* **2017**, *201*, 150-158.